

Flow and dispersion in coupled outdoor and indoor environments: issue of Reynolds number independence

Yuwei Dai^a, Cheuk Ming Mak^{a *}, Zhengtao Ai^b

^a Department of Building Services Engineering, The Hong Kong Polytechnic University, Hong Kong, China

^b International Center for Indoor Environment and Energy, Department of Civil Engineering, Technical University of Denmark

*Corresponding author: Cheuk Ming Mak, Department of Building Services Engineering, The Hong Kong Polytechnic University, Hung Hom, Kowloon, Hong Kong. Email: cheuk-ming.mak@polyu.edu.hk

Abstract

The Reynolds number (Re) independence criteria for flow and dispersion around purely outdoor environments has been examined in many previous studies, but little attention has been paid to the coupled outdoor and indoor environments. This study investigated the Re independence criteria of flow and dispersion in coupled outdoor and indoor environments using Computational Fluid Dynamics (CFD) with Large Eddy Simulation (LES) model. Two geometrical arrangements were considered, namely an isolated multi-story building, and an array of multi-story buildings. Four parameters including the non-dimensional air velocity, pollutant concentration, ventilation rate, and re-entry ratio were used to assess the Re independence criteria. The tracer gas decay method was used to predict the ventilation rate and to quantify the re-entry ratio for each room. Using the quantitative indicator, the deviation rate (DR), of the non-dimensional velocity below 5%, two sets of critical values were proposed: Re_H based on the building height equal to 4.8×10^4 for the outdoor environment, and Re_W based on the opening height equal to 1.4×10^4 for the indoor environment. The concentration field was more difficult to meet the Re -independent requirement. Using the DR of the non-dimensional concentration below 5%, the critical values were $Re_H = 7.9 \times 10^4$ and $Re_W = 3.0 \times 10^4$. If the DR was enlarged to 10%, the Re_H and Re_W criteria for the concentration field were the same as the velocity fields. For the non-dimensional ventilation rate and re-entry ratio, the critical value for the Re independence was $Re_W = 1.4 \times 10^4$ for both the isolated buildings and the building arrays.

Keywords: Reynolds number independence criteria, coupled outdoor and indoor environment, natural ventilation, pollutant dispersion, CFD simulation.

1. Introduction

As it is associated strongly with human health, the dispersal of pollutants in urban environments has attracted special attention. There is a large amount of literature addressing pollutant dispersion in either purely outdoor environments, or purely indoor environments. An increasing number of studies [1-12] have investigated the dispersion in coupled indoor and outdoor environments, because substantial evidence indicates that numerous sources of air pollution, such as traffic exhaust, dust, pollen, airborne viruses, and toxic and odorous emissions, travel from the outdoor to the indoor environments [13]. Particularly, the SARS outbreak in Hong Kong demonstrated that virus-laden expiratory droplet nuclei can be transported between floors through open windows [2, 14]. Therefore, an accurate and reliable investigation of flow and dispersion in coupled outdoor and indoor environments is of great importance.

Several methods have been used to investigate air flow aerodynamics and air pollutant dispersion including field measurements, wind tunnel experiments, and Computational Fluid Dynamics (CFD). Full-scale field measurements consider all phenomena related to the airflow and dispersion fields under real atmospheric conditions. However, field measurements have certain limitations and difficulties such as limited data collection positions and uncontrolled wind and weather conditions. Unlike field measurements, wind tunnel experiments allow to a large extent control over the boundary conditions. However, restricted by physical boundaries, reduced-scale models are generally used for wind tunnel tests, which may cause the similarity problem [15, 16]. It also suffers from the limited number of measurement points. Compared to field tests and wind tunnel experiments, CFD simulations have certain advantages such as the ability to fully control the boundary conditions and provide whole flow field data without limitations [17]. In addition, reduced-scale models have also been used in a large number of CFD studies to investigate the flow structure and pollutant dispersion in urban environments to save computational resources. It has been proven that the reduced-scale models in CFD modelling can also acquire accurate predictions and save very large computational costs [18]. However, using reduced-scale models in CFD simulations carries the same disadvantages and limitations as reduced-scale wind tunnel experiments. In addition, it should be noted that CFD models were developed based on simplifications and assumptions, and therefore, careful validation against experimental data is an essential part of any CFD study.

The main problem with adopting reduced-scale models in both wind tunnel experiments and CFD simulations is the difficulty of achieving similarity requirements. Pointed out by Snyder [16], one of the most important criteria for simulating isothermal flow and dispersion fields is the Reynolds number (Re) independence. According to Re -independence theory, when the Re exceeds a critical value, the flow field would enter an Re -independent regime and the flow characteristics do not change with the increase of Re [16]. Several diverse critical Re values have been proposed in previous studies from wind tunnel measurements. Most of them range from 2×10^3 to 1×10^5 [16, 19-24]. More recently, Cui et al. [25, 26] determined the critical Re value as 3.3×10^4 based on the characteristic height of the building by CFD simulations. In addition, Cui et al. [26] summarized several types of Re and critical values from the literature, including building Re and roughness Re . Most previous studies on the Re -independence problem investigated the flow around purely outdoor environments, however, the Re -independence of pollutant dispersion and of indoor environments needs to be fulfilled, especially for coupled outdoor and indoor issues that are more difficult to meet the similarity requirements. Typical examples of such coupled indoor and outdoor issues are natural ventilation and pollutant dispersion between rooms in urban environments [18].

In natural ventilation studies, buildings located in urban environments contain multiple different geometrical length scales between the urban area ($1 - 1.5 \text{ km}$) and ventilation openings ($0.01 - 1 \text{ m}$) [27]. The large differences make the normal Re criteria ($Re = U_{ref} \cdot H/\nu$), such as 1.5×10^4 based on the building height (H) for a reduced-scale model [16], unsuitable for ventilation studies. Using an opening with the full-scale dimensions of $1 \text{ m} \times 1 \text{ m}$ as an example, at a scale of $1 : 100$, the reduced-scale dimensions should be $10 \text{ mm} \times 10 \text{ mm}$. The Re of the opening is only around 3000 even based on a velocity of 5 m/s , while it is 3.3×10^5 at full scale. This discrepancy will change the flow regime through the reduced-scale openings from a fully turbulent flow to a transitional flow, or even laminar flow, and this would obviously contravene the similarity law [18, 27]. Suggested by Cermak et al. [28], an Re based on the maximum velocity and the minimum dimension of an opening should exceed 2×10^4 in wind tunnel experiments. Similar to wind tunnel tests, the reduced-scale models in CFD simulations should be unsuitable for investigating ventilation problems if they disobey the similarity criteria. However, in previous studies investigating reduced-scale

ventilation issues, most have used the building-height-based Re criteria of purely outdoor environments to claim the independence of similarity [3-5, 7-10, 29-31] and therefore lack authenticity and accuracy.

Regarding natural ventilation problems, the ventilation rate, or air changes per hour (ACH) is one of the most important parameters used to evaluate the ventilation efficiency of a specific room. A comprehensive overview of the ventilation assessment approaches was presented by Chen [32] that concluded about 70 percent of the ventilation studies were conducted using CFD models. More recently, Ai and Mak [33, 34] used CFD methods to analyze multiple influences on the ventilation rate based on a full-scale single-sided room. In their study, two calculation methods were compared, the integration method and tracer gas decay method, and the latter was revealed to yield better results. However, only a few of the previous studies [1] employed the tracer gas decay method to investigate the ACH in multistory buildings because of the huge numerical costs. In addition, the Re will significantly affect the accuracy of the prediction of ventilation rates for each room in a reduced-scale multistory building model if the similarity requirement is not fulfilled. Therefore, a detailed investigation of the Re -independence of the ventilation rate in such coupled indoor and outdoor environment is needed.

Since the pollutant dispersion in coupled outdoor and indoor transportation typically depends on the flow structure and ventilation efficiency of each room, the accurate prediction of pollutant transportation in reduced-scale models relates closely to the authentic flow fields and ventilation rates. In the real urban environment, a number of factors will affect the wind flow fields and ventilation performance of the rooms, but this study only considered the wind-driven flow to investigate the similarity requirements. Therefore, the objective of this study was to investigate the Re -independence criteria of isothermal flows and pollutant dispersions in reduced-scale multistory buildings. Two typical geometrical arrangements were considered: an isolated building and building arrays. The tracer gas technique, using carbon dioxide (CO_2), was adopted to simulate the concentration decay and the gaseous pollutant dispersion. This study intends to provide detailed criteria of Re -independence for future wind tunnel experiments and CFD practices to acquire more precise flow field and pollutant dispersion estimations. Section 2 introduces the CFD method, and the validation process is elaborated in Section 3. Section 4 presents the configuration descriptions of the current models, and detailed analysis of the results are presented in Section 5. Section 6 summarizes and concludes the study.

2. Methodology

2.1 CFD model

In order to generate the instantaneous flow fields, a Large Eddy Simulation (LES) was used to predict the airflow fields and the tracer gas concentration decay. The governing equations in the LES models for the incompressible Newtonian fluids were obtained as follows:

$$\frac{\partial \bar{u}_i}{\partial x_i} = 0, \quad (1)$$

$$\frac{\partial(\rho \bar{u}_i)}{\partial t} + \frac{\partial(\rho \bar{u}_i \bar{u}_j)}{\partial x_j} = -\frac{\partial \bar{p}}{\partial x_i} + \vartheta \frac{\partial^2 \bar{u}_i}{\partial x_i^2} - \frac{\partial \tau_{ij}}{\partial x_j}, \quad (2)$$

$$\frac{\partial(\rho \bar{c})}{\partial t} + \frac{\partial(\rho \bar{u}_j \bar{c})}{\partial x_j} = -\frac{\partial J_j}{\partial x_j}, \quad (3)$$

where the overbars ($\bar{\quad}$) indicate the filtered variables, u_i and u_j represent the velocity components, p represents the pressure, ρ represents the density, ϑ represents the viscosity, and c represents the tracer gas concentration (ppm).

During the filtering process, the terms τ_{ij} and J_j appear in the momentum and concentration equations that are the subgrid-scale (SGS) stresses defined as:

$$\tau_{ij} = \rho \overline{u_i u_j} - \rho \overline{u_i} \overline{u_j}, \quad (4)$$

$$J_j = \overline{u_j c} - \overline{u_j} \overline{c}, \quad (5)$$

These terms represent the impact of the non-resolved small-scale eddies on the large-scale eddies. In order to close the governing equations, the Boussinesq hypothesis [35] was used to correlate the term τ_{ij} with the strain rate tensor $\overline{S_{ij}}$, defined by:

$$\tau_{ij} - \frac{1}{3} \tau_{kk} \sigma_{ij} = -2\mu_t \overline{S_{ij}}, \quad (6)$$

$$\overline{S_{ij}} = \frac{1}{2} \left(\frac{\partial \overline{u_i}}{\partial x_j} + \frac{\partial \overline{u_j}}{\partial x_i} \right), \quad (7)$$

where μ_t represents the subgrid-scale turbulent viscosity, and the isotropic variable τ_{kk} is zero for incompressible flows. In this study, the Smagorinsky–Lilly model [36, 37] was used to model the μ_t and μ_t terms calculated as:

$$\mu_t = (C_s \Delta)^2 \sqrt{2 \overline{S_{ij}} \overline{S_{ij}}}, \quad (8)$$

where the Smagorinsky constant C_s is empirically given as 0.1, and Δ represents the grid scale.

2.2 Solution method

The numerical simulations were performed using Fluent 13.0 [38] with the finite volume method. The initial condition for each unsteady case is the converged mean flow field generated by a RANS model (RNG $k - \varepsilon$). The unsteady flow and concentration fields were generated simultaneously. The discretization methods for the pressure and diffusive terms used a second-order upwind scheme, whereas the second-order bounded central-differencing scheme was used for the convective term. A second-order implicit scheme was used for the temporal discretization. The pressure-velocity coupling SIMPLEC method was used. The time step size was set as $\Delta t = 0.01s$ and all cases were calculated until the residuals were less than 10^{-5} , and the convergence of each time step was achieved when both the spatially averaged wind speed at the monitor points and the test room CO_2 concentrations were stable for at least 10 iterations.

2.3 Calculation of single-sided ventilation

In this study, the tracer gas decay method was adopted to calculate the ventilation rate of a specific room. Assuming there was neither a background concentration nor an indoor tracer gas source, the ventilation rate (Q_t) (m^3/s) during a sub-period of $\Delta t = t_{i+1} - t_i$ can be calculated using a two-point method [39] as:

$$Q_t = \frac{\ln(C_{t_i}/C_{t_{i+1}})}{t_{i+1} - t_i} \cdot V \quad (9)$$

where C_{t_i} and $C_{t_{i+1}}$ represent the spatially averaged tracer gas concentrations (ppm) of the room at time t_i and t_{i+1} (s), respectively, and V represents the volume of the room (m^3). The CFD simulation can easily use the time step size, which is the temporal discretization interval, as the sub-period Δt to determine Q_t . As a result, Q_t can be termed as the instantaneous ventilation rate at the time t . The averaged ventilation rate (\overline{Q}) in the overall decay period is then calculated by:

$$\overline{Q} = \frac{\sum_{i=0}^n Q_t}{n} \quad (10)$$

where n represents the number of sub-periods. In this study, the ventilation rate for each case was converted to the air exchange per hour (ACH) (h^{-1}) for comparison convenience as:

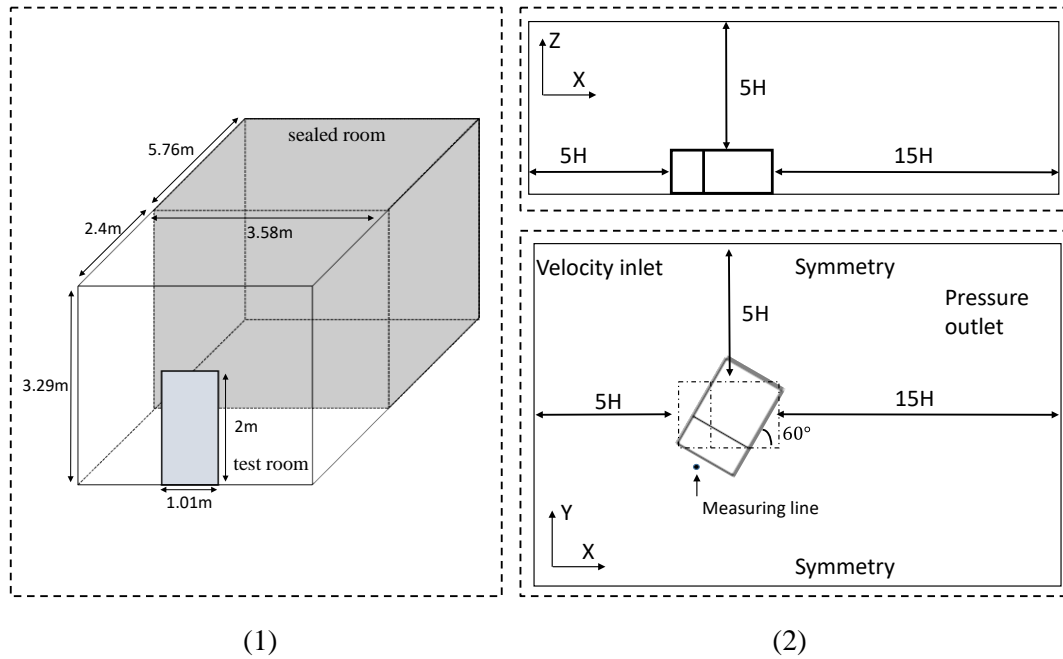
$$ACH = \frac{\bar{Q}}{V} \cdot \frac{3600}{t} \quad (11)$$

3. Validation of CFD method

3.1 Validation of the ventilation rate

This study adopted the full-scale building model of the field measurements taken by Dascalaki [40] to validate the CFD prediction for the ventilation rate. The geometry description of the building model is shown in Fig. 1(1). The building model contained two rooms: a test room with a single-sided opening and a preparation room that was sealed during the measurement. The preparation room was set as a solid block in the current CFD simulations. This field measurement was conducted under a mean incident wind angle of 60° (0° for a normal incidence) and a mean inflow velocity of $1.95 \pm 0.52 \text{ m/s}$ at a height of 1.5 m . Dascalaki and his co-workers used the concentration decay method with NO_2 as the tracer gas to measure the ventilation rate through the single-sided opening.

In the validation simulations, a wind speed of 1.95 m/s at 1.5 m was adopted. The computational domain of this model was built with an upstream length of $5H$, a downstream length of $15H$, a lateral length of $5H$, and a height of $5H$, as shown in Fig. 1(2). The inlet wind flow was at the incident direction and the building model was rotated with an angle of 60° to the normal incidence. The domain was built according to the best-practice guidelines to ensure accurate flow development. The blockage ratio of the domain size was 1.4% which is lower than the recommended value (3%) [41]. Three mesh systems using coarse, medium, and fine structured hexahedral cells were constructed with near-wall minimum grid widths of 0.01 , 0.005 , and 0.003 m , respectively; the mesh arrangements are shown in Fig. 1(3). The grid numbers were around 3.34 , 4.2 , and 5.1 million, respectively. Fig.1 (4) shows the mesh sensitivity test for the non-dimensional wind velocity at a vertical line in front of the building. The 0.01 m mesh system results displayed considerable underestimations compared to the others, while the 0.005 m and 0.003 m results were basically equivalent. Therefore, the medium mesh system with 4.2 million grids was selected for the ACH simulation.



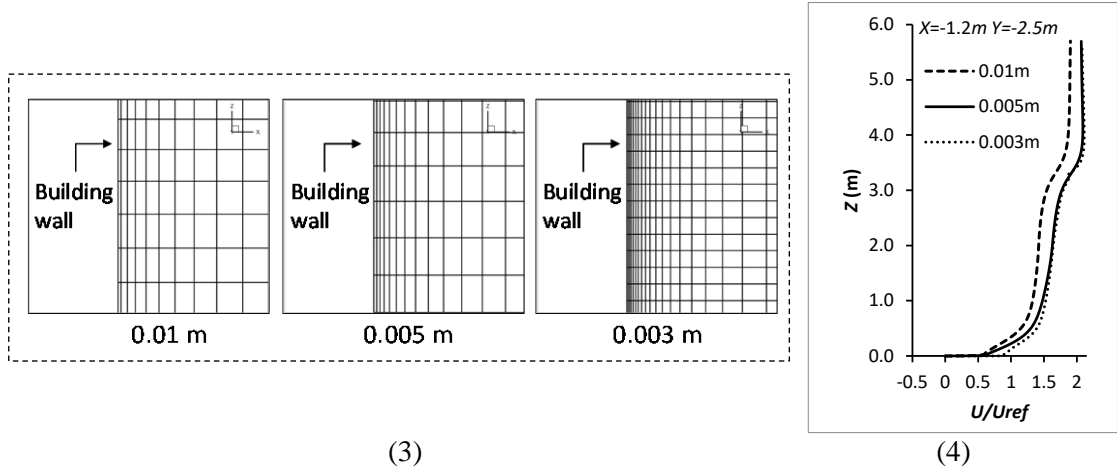


Fig. 1 (1) Building model dimensions; (2) Computational domain: side view and top view; (3) Near-wall mesh arrangement of the three systems; (4) Sensitivity test for the three mesh systems at line $X = -1.2 \text{ m}$, $Y = -2.5 \text{ m}$, and the position shown in (2).

The RNG $k - \varepsilon$ model was used to construct the initial steady flow field. The inlet boundary conditions of the domain was shown in Table 1 to perform the initial flow field which followed the logarithm law by the profiles of the mean wind speed U , turbulent kinetic energy k , and turbulent dissipation rate ε . The coefficients listed in Table 1 are: $z_0 = 0.000255 \text{ m}$, $u^* = 0.0941 \text{ m/s}$, $C_1 = 0.025$, and $C_2 = 0.41$. In addition, the Von Karman constant κ was 0.4187 and $C_\mu = 0.002$. For the unsteady simulation of the tracer gas concentration in the LES model, the turbulent Schmidt for the SGS motions (Sc_{SGS}) of 0.4 was used.

Table 1. Boundary conditions

	Power law type
Domain inlet	$U = \frac{u^*}{\kappa} \ln \left(\frac{z + z_0}{z_0} \right)$ $k = \sqrt{C_1 \cdot \ln(z + z_0) + C_2}$ $\varepsilon = \frac{u^* \sqrt{C_\mu}}{\kappa(z + z_0)} \sqrt{C_1 \cdot \ln(z + z_0) + C_2}$
Domain outlet	$\frac{\partial}{\partial x}(u, v, w, k, \varepsilon) = 0$
Domain ceiling	$w = 0, \frac{\partial}{\partial x}(u, v, k, \varepsilon) = 0$
Domain lateral sides	$v = 0, \frac{\partial}{\partial x}(u, w, k, \varepsilon) = 0$
Domain ground	Enhanced wall functions
Building surfaces	Non-slip for wall shear stress
Turbulence model coefficients	$C_\mu = 0.002, \kappa = 0.4187$

The sensitivity of the selected length of the sub-period Δt concerning the prediction of the averaged ventilation rate was constructed. Different time intervals of 0.005 s, 0.01 s, 0.1 s, 1 s, and 3 s were adopted to compare the prediction of the mean ACH values. For each time interval simulation case, the decay time was greater than 40 s for the ventilation rate calculations. The results are shown in Table 2. The predicted ACH values of different sub-periods were essentially consistent with the experiment results, except for the value of $\Delta t = 3 \text{ s}$, that was slightly overestimated. However, pointed by Ai and Mak [34], the averaged predicted ACH values were roughly independent of the time interval. This discrepancy may be attributed to the fact that $\Delta t = 3 \text{ s}$ is in the middle of the periodic wind gust timing that affects the accuracy of the tracer gas movement behavior prediction. However, for the overall ACH of a room, this discrepancy was not large. Generally, the LES model using the tracer gas decay

method predicted good results for the ventilation rate of a single-sided opening room, and $\Delta t = 0.01$ s was adopted to calculate the ACH values in the later simulation.

Table 2. Comparison of the predicted and measured ACH results

Δt (s)	0.005	0.01	0.1	1	3	Measurements
ACH (h^{-1})	11.68	11.54	12.01	12.45	13.4	11.39 ± 1.79

3.2 Validation of the flow field and concentration dispersion

As the full-scale experiment described in Section 3.1 provides the results only for the ACH, the flow and concentration fields with the CFD simulation were justified by a 1:200 wind tunnel experiment [42]. The flow and dispersion fields in the 3×7 rectangular building array models (CEDVAL B1-1) were measured in the Blasius wind tunnel at the University of Hamburg. The geometric description is shown in Fig. 2(1). The target building had four pollution sources with an emission speed of 0.025 m/s on the leeward wall, as shown in Fig. 2(2). The airflow and concentration fields were measured by the Laser Doppler Velocimetry (LVD) technique and a Flame Ionization Detector (FID), respectively. The same numerical method as the validation in Section 3.1 was used, except for the lateral distance of the computational domain that was $3.4 H$ based on the wind tunnel width. The boundary conditions from Table 1 were used to generate the inlet flow, and based on the experimental data, the coefficients in Table 1 changed as $z_0 = 0.00075$ m, $u^* = 0.4078$ m/s, $C_1 = 0.025$, $C_2 = 0.41$, $\kappa = 0.4187$, and $C_\mu = 0.069$. The initial steady flow was simulated using the RNG $k - \varepsilon$ model, then the transient airflow and concentration fields were predicted by the LES model at the same time.

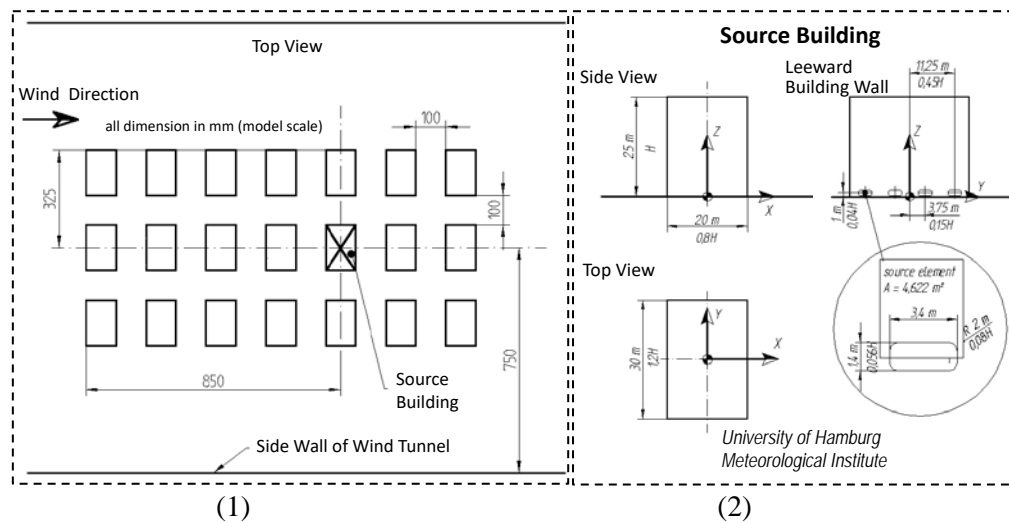


Fig. 2 (1) Dimensions of the building arrays, (2) the source building, and source [42].

The simulated results from the wind velocity and the pollutant dispersion are shown in the Fig. 3, the concentration value was calculated in the non-dimensional form as $K_c = \frac{C_{local}}{C_{source}} \cdot \frac{U_{ref} H^2}{Q_{source}}$, where C_{local} is the measured concentration (ppm), C_{source} is the concentration (ppm) at the source, U_{ref} is the reference wind speed (m/s) (6 m/s), H is the building height ($H = 0.125$ m), and Q_{source} is the flow rate of the source emission (m^3/s). As shown in Fig.3, the CFD results agree well with the experimental data regarding wind flow velocity and the concentration dispersions. Therefore, the LES model can be justified to produce accurate airflow and concentration fields in the building arrays. The details of this validation are given in our previous study [43].

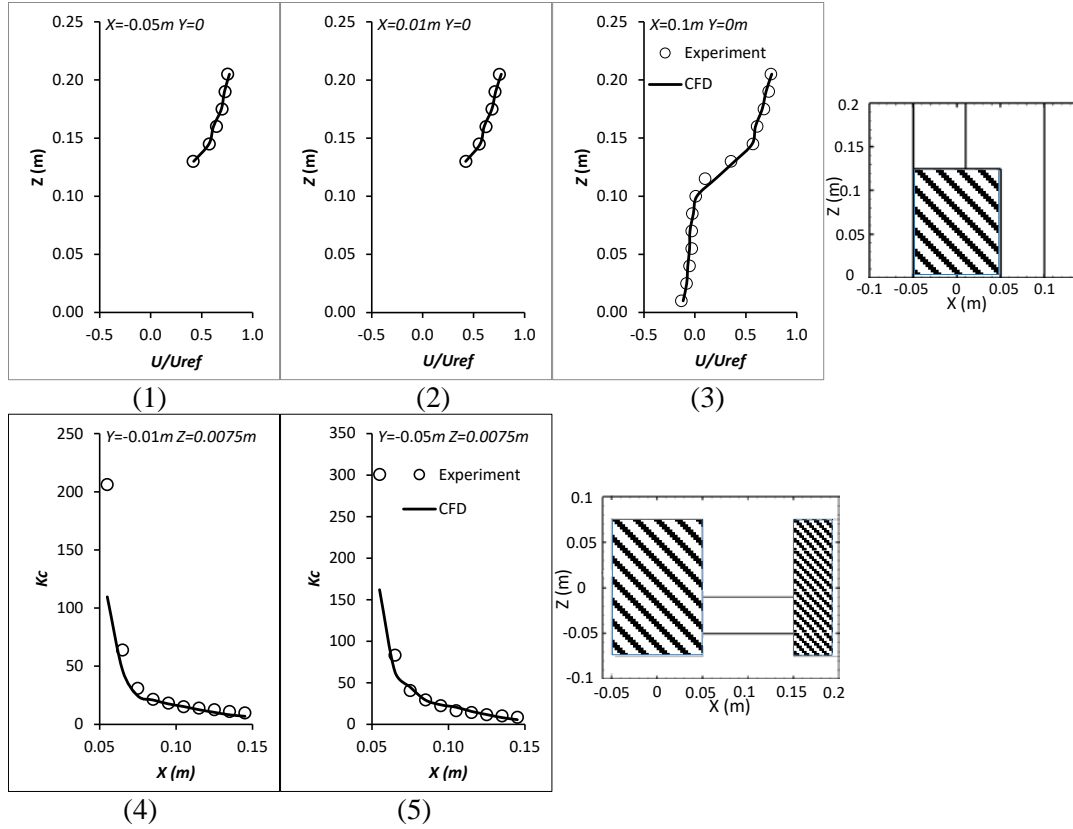


Fig. 3 The mean wind velocity and concentration distribution of the simulated and experimental results. (1)–(3) The mean velocity distribution and the compared locations. (4)–(5) The mean concentration distribution and the compared locations.

4. Configuration descriptions

In order to investigate the Re -independence requirements for the flows and pollutant dispersions in the coupled indoor and outdoor environment, two 1:10 reduced-scale building models were constructed: case A, an isolated four-story building; case B, a 3×5 array of buildings with one target four-story building. The building dimensions are shown in Fig.4. Each building had a length \times width \times height = $0.5\text{ m} \times 0.5\text{ m} \times 1.2\text{ m}$, the windward opening dimension of the target building was length \times height = $0.25\text{ m} \times 0.15\text{ m}$, and the open area over each floor was 0.075 m . Note that this open area dimension is larger than most real windows, however, this should not influence the examination of the Re -independence. For the building arrays, the distance between the neighboring building was 0.5 m . The computational domain of the two cases was constructed following the validation in Section 3.1 and the domain of the building arrays is shown in Fig. 4(2). The boundary conditions were adopted from Table 1, except for the inlet boundary conditions. The wind direction was perpendicular to the inlet plane and the opening of the room. In order to change the Re number, the inlet wind flow profiles were varied from 0.2 m/s to 5 m/s . The detailed information is given in Table 3, and the U_{ref} was the referenced wind velocity at the top of the building, Re_H was calculated based on the characteristic height of the building, and Re_W was based on the height of the window. In order to calculate the ventilation rates, each case was calculated for more than 60 s of the concentration decay.

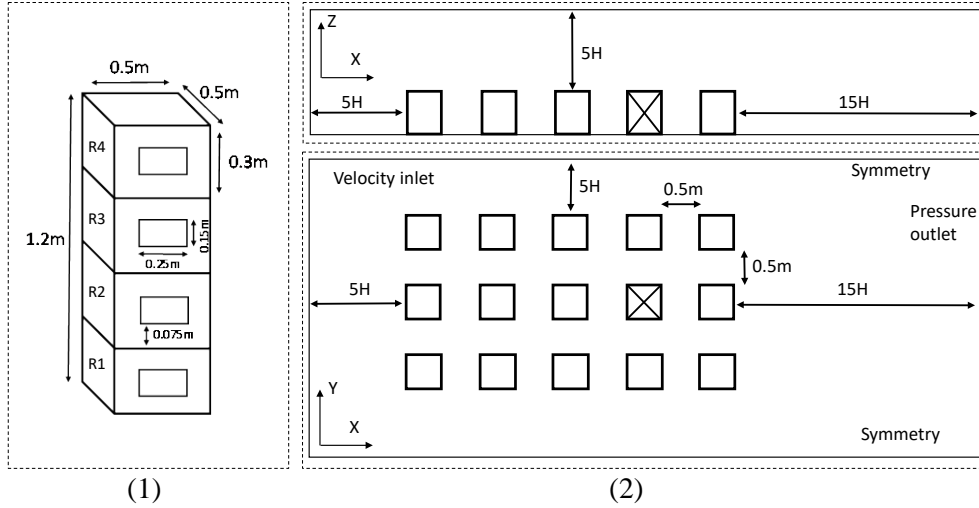


Fig. 4 (1) Dimensions of the isolated building and the target building in the arrays. (2) The arrangement and computational domain of the building arrays with a side view and top view.

Table 3. Reynolds number according to the reference velocity.

U_{ref} (m/s)	Re_H	Re_W
0.2	15882 (1.6×10^4)	1985 (0.2×10^4)
0.6	47647 (4.8×10^4)	5956 (0.6×10^4)
1.0	79412 (7.9×10^4)	9927 (1.0×10^4)
1.4	111177 (1.1×10^5)	13897 (1.4×10^4)
2.0	158825 (1.6×10^5)	19853 (2.0×10^4)
3.0	238237 (2.4×10^5)	29780 (3.0×10^4)
4.0	317649 (3.2×10^5)	39706 (4.0×10^4)
5.0	397062 (4.0×10^5)	49633 (5.0×10^4)

5. Results and discussion

5.1 An isolated building

5.1.1 Airflow field

The comparisons of the non-dimensional averaged wind speeds (U/U_{ref}) of the outdoor and indoor environments are shown in Figs. 5(1)–(7) separately. The relative positions of the measured lines are shown in Fig. 5(3). Figs. 5(1)–(3) show the velocity fields at three vertical lines near the building, and it is clearly shown that when the Re_H was larger than 4.8×10^4 (U_{ref} is 0.6 m/s), the non-dimensional wind velocity discrepancies become insignificant with increases in the Re_H . When the Re_H was smaller than 4.8×10^4 (U_{ref} was less than 0.6 m/s), the main differences occurred on the top and leeward side of the building as shown in Figs. 5(1)–(3). This means that the turbulent flow characteristics on the roof and leeward wall of the isolated building cannot be similarly reconstructed. Figs. 5(4)–(7) show the velocity distributions at a vertical line in four rooms, respectively, and the mean wind velocity distributions of the Re_W less than 0.6×10^4 (U_{ref} is 0.6 m/s) display obvious divergences compared to those larger than 1×10^4 . This reveals that the indoor airflow fields are drastically changed with an increase of the Re_W from 0.2×10^4 to 1.4×10^4 . In addition, it may exist a critical value of Re_W to ensure reconstruction of the indoor airflow distributions which needs to be quantitatively assessed later. It also reveals that the critical Re value should be different in the outdoor and indoor environments.

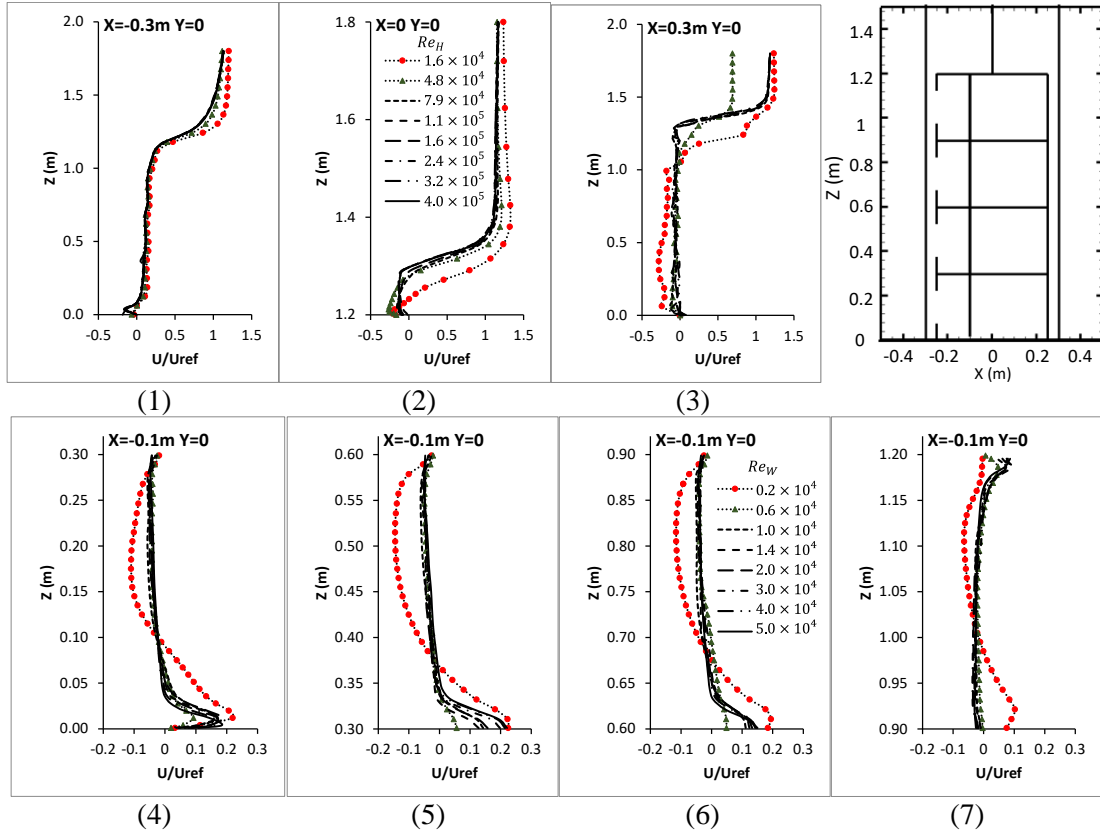
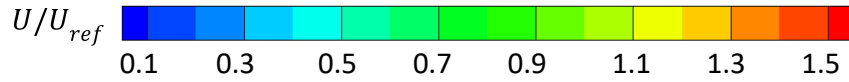


Fig. 5 Comparisons of the non-dimensional velocity on the outdoor and indoor environments. (1) - (3) Velocity distribution of the outdoor field, and the (4) - (7) velocity distribution of the indoor field.

Similar observations can be made from the non-dimensional velocity vectors of the vertical plane $Y = 0$, as shown in Fig. 6. For the outdoor environment, the reattachment on the roof of the building was not apparently reconstructed when the Re_H was smaller than 4.8×10^4 , but a small vortex occurred on the leeward side of Room 4 as shown in Figs. 6(1) and (2). However, when the Re_H was larger than 7.9×10^4 , the airflow distributions around the top of the building were basically analogous, including the reattachment on the roof and the upward wind on the leeward side of the building. For the indoor environment, multiple vortices were formed in Room 4 as shown in Figs. 6(1) and (2), with the increase of the Re_W , the number of vortices decreased and the averaged wind field became more stable. When the Re_W was larger than 1.4×10^4 , the indoor airflow field was characterized by a large recirculation with the core of the recirculation in the latter half of Room 4, although the exact positions of the vortices were slightly different.



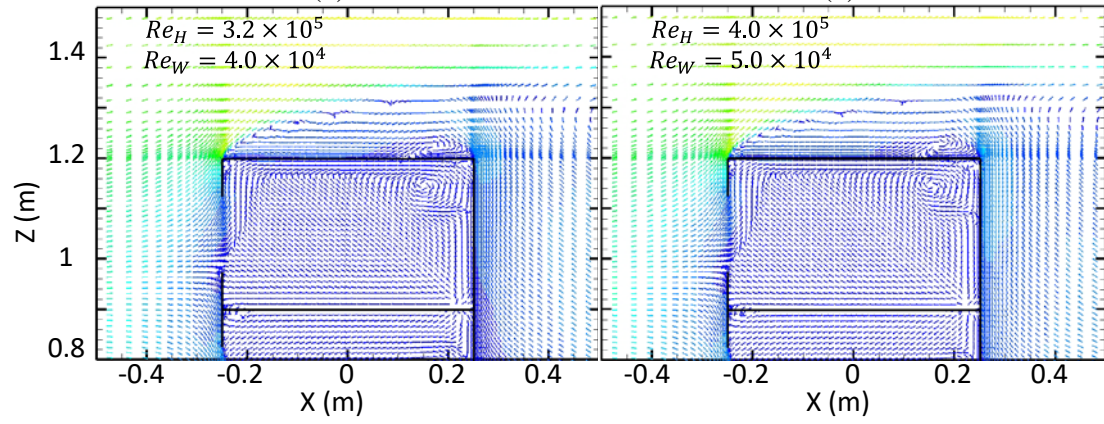
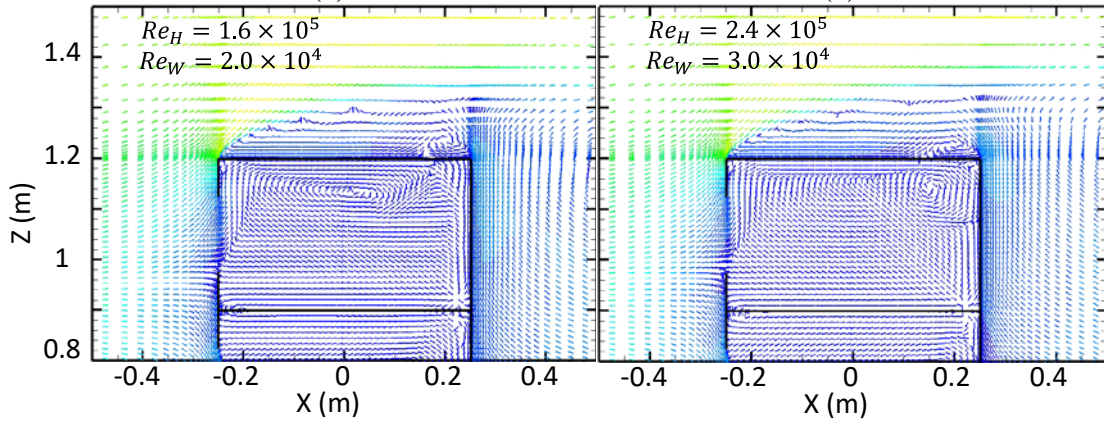
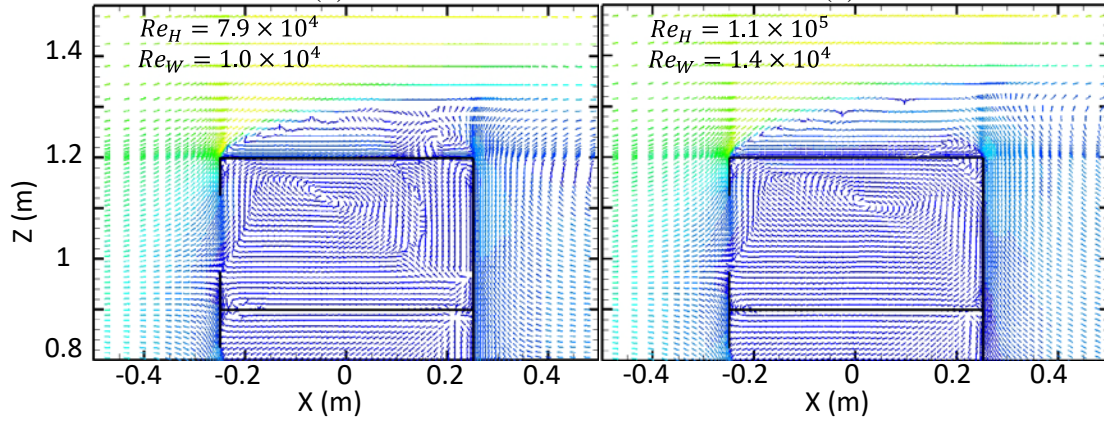
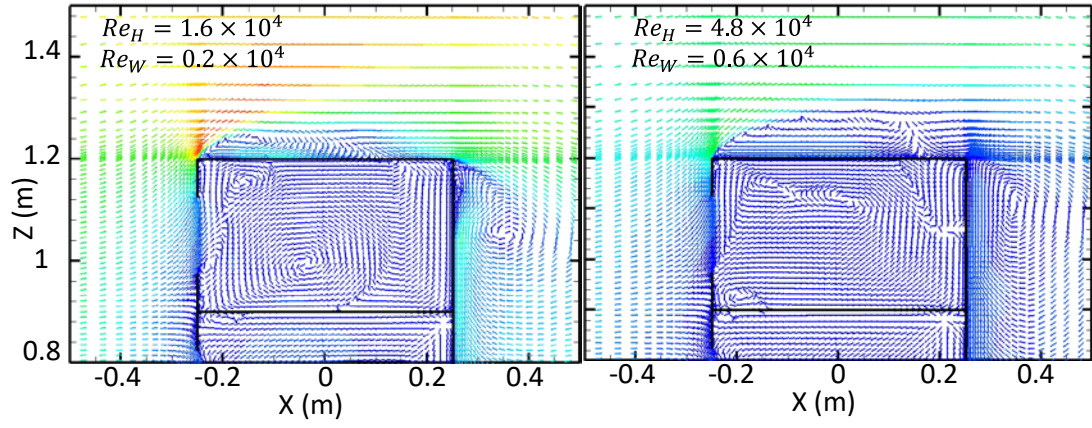


Fig. 6 Comparisons of non-dimensional velocity vectors on the vertical plane $Y = 0$ of the outdoor and indoor environments with variations of Re_H and Re_W .

In order to quantitatively determine the critical Re value for both the indoor and outdoor environments, a quantity of the deviation rate is proposed to evaluate the Re -independence feature. The deviation rate, which is the ratio of changes to the dimensionless velocity with different Re , is calculated as:

$$DR = \left| \frac{U^*_{Re_i} - U^*_{Re_j}}{U^*_{Re_i}} \right| \quad (12)$$

where U^* is the non-dimensional velocity (U/U_{ref}) according to changes in the Re and Re_i , and Re_j is the different levels of the Re . When the deviation rate is less than a specific value, the differences of the flow fields will be insignificant. Previous studies [25, 26] suggested the variation of the relative changes should be less than 5%. This study also used 5% as the indication, meaning that when $DR \leq 5\%$, the flow characteristics will be termed as the Re -independent flow.

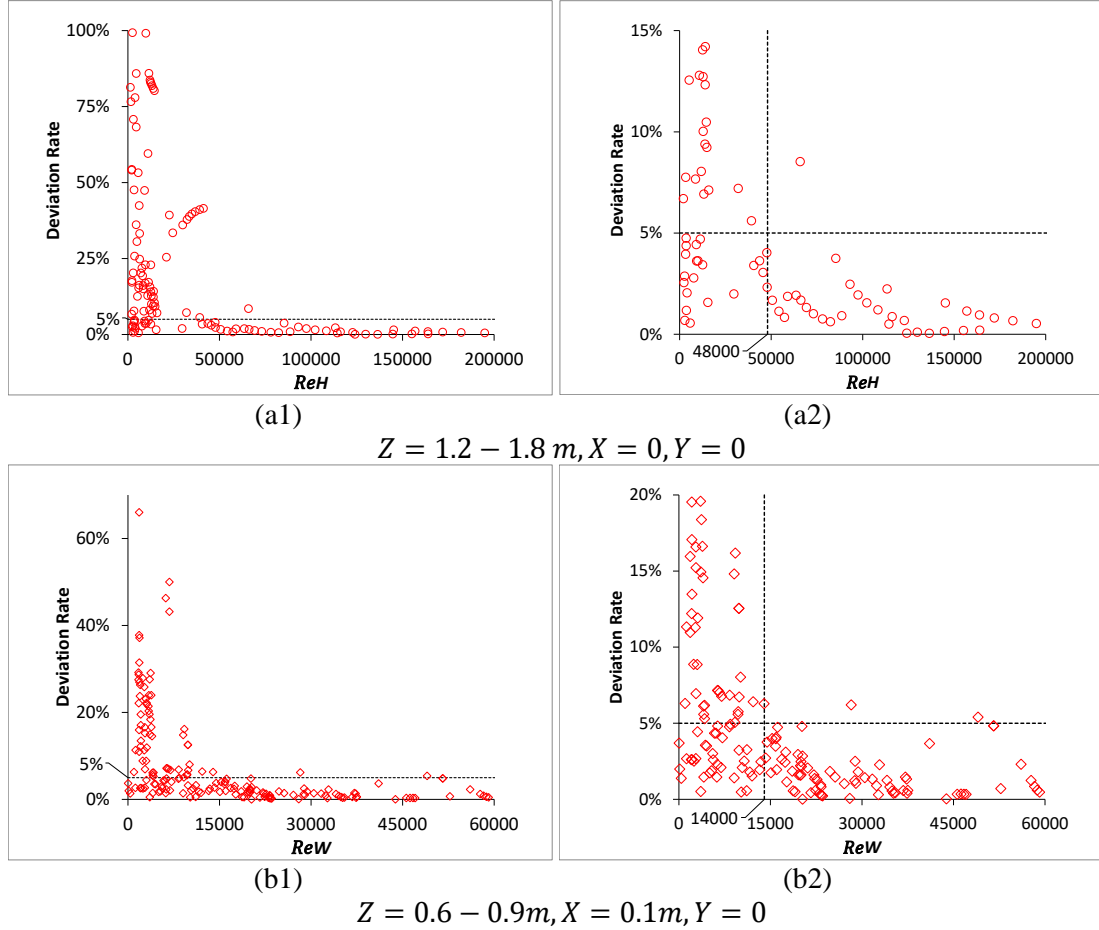


Fig. 7 DR variations for the averaged non-dimensional velocity with changes in the Re_H and Re_W . (a1) and (a2) The outdoor environment against the Re_H , and (b1) and (b2) the indoor environment against the Re_W . (a1) and (b1) are the amplified values in (a2) and (b2).

Fig. 7 displays the DR results after varying the Re_H and Re_W of the outdoor and indoor environments, respectively. The outdoor Re was calculated based on the mean wind velocity and the heights of the building for each measuring point. The indoor Re was comparable to the Re_W level since the indoor area was the low- Re regime. Two findings can be noted from Fig. 7. First, the data scatter for both outdoor and indoor conditions revealed an acute decrease in

the DR when the Re was larger than a certain value. Also, with the Re larger than a certain value, the DR differences became smaller and the decreasing trend became milder. The DR remained below 5% except for a few outliers. Second, the outdoor and indoor conditions did not have comparably critical Re . A DR value lower than 5% in the outdoor condition was associated with an $Re_H > 4.8 \times 10^4$, while with an $Re_W > 1.4 \times 10^4$ for the indoor condition the Re_H was 1.1×10^5 . This discrepancy reveals that the indoor environment had stricter requirements to reach the Re -independence situation. Considering the air flow structures shown in Fig. (6), two sets of critical Re were suggested: $Re_H = 4.8 \times 10^4$ based on the building height for the outdoor situation and $Re_W = 1.4 \times 10^4$ based on the opening height for the indoor situation according to the rough values from Table. 3.

5.1.2 Concentration field

In order to predict the ventilation rate using the concentration decay method, each room was initially filled uniformly with the tracer gas (CO_2) and the initial concentration of each room was 75 g/m^3 . As the tracer gas decays, it can not only be used to calculate the air exchange rate in each room, but also as the pollution source. Therefore, the concentration value was obtained in a non-dimensional form as:

$$K = \frac{C_{local}}{(C_{room T_0} - C_{room T_1}) \cdot V / A_W} \quad (13)$$

where C_{local} is the measured concentration (g/m^3) of tracer gas, $C_{room T_0}$ is the concentration (g/m^3) of the source room at the beginning, $C_{room T_1}$ is the concentration (g/m^3) of the source room at time T_1 , V is the volume of the room (m^3), and A_W is the area of the window (m^2).

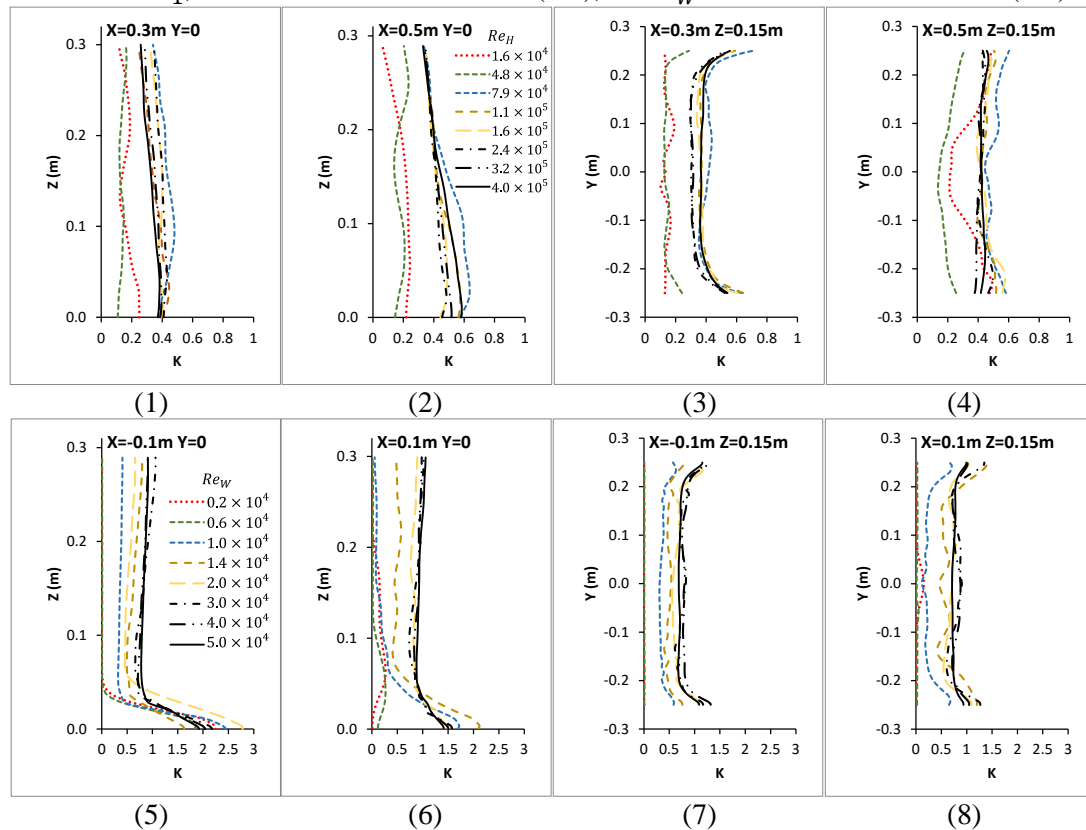


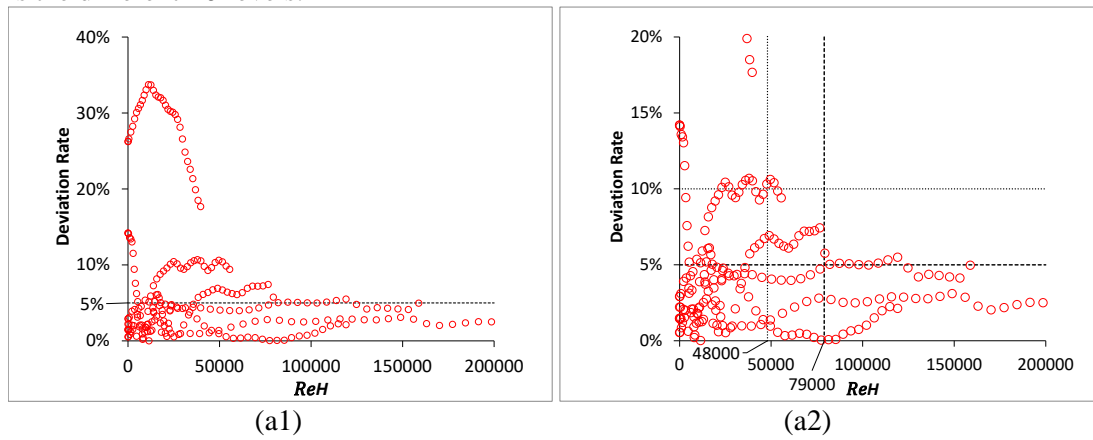
Fig. 8 Comparisons of the non-dimensional concentration on the outdoor and indoor environments at lines of the vertical ($Y = 0$) and horizontal plane ($Z = 0.15m$). (1)–(4) Concentration distribution of the outdoor field and the (4)–(7) concentration distribution of the indoor field.

Assuming Room 2 (R2) as the source room filled with tracer gas (CO_2), after a sampling period, the tracer gas was mainly transported downward into Room 1 (R1) and to the leeward side of the building. Figs. 8(1)–(8) display the comparisons of the non-dimensional concentration on the outdoor and indoor environments at lines of both vertical ($Y = 0$) and horizontal directions ($Z = 0.15\text{ m}$), with the referenced wind velocity varying from 0.2 m/s to 5 m/s . For the outdoor environment, because of the relatively small value of the concentration results, the differences in the concentration results with an increase in the Re_H were not very large except for the distinguishable underestimations for the $Re_H < 4.8 \times 10^4$ ($U_{ref} < 0.6\text{ m/s}$). Also, the results of the $Re_H = 7.9 \times 10^4$ ($U_{ref} = 1.0\text{ m/s}$) showed minor overestimations compared to those of the Re_H over 1.1×10^5 , as shown in Figs. 8(1) - (4). However, for the indoor environment, the pollutant distribution displayed more complex behaviors. Considerable differences were detected from the Re_W values less than 1.4×10^4 (U_{ref} less than 1.4 m/s) in both the vertical and horizontal directions. When the Re_W was larger than 2×10^4 , the changing rate decreased and the distribution patterns of the non-dimensional concentration remained similar. Considering both the outdoor and indoor pollutant dispersion fields, this illustrates that critical values for the outdoor and indoor Re should be different.

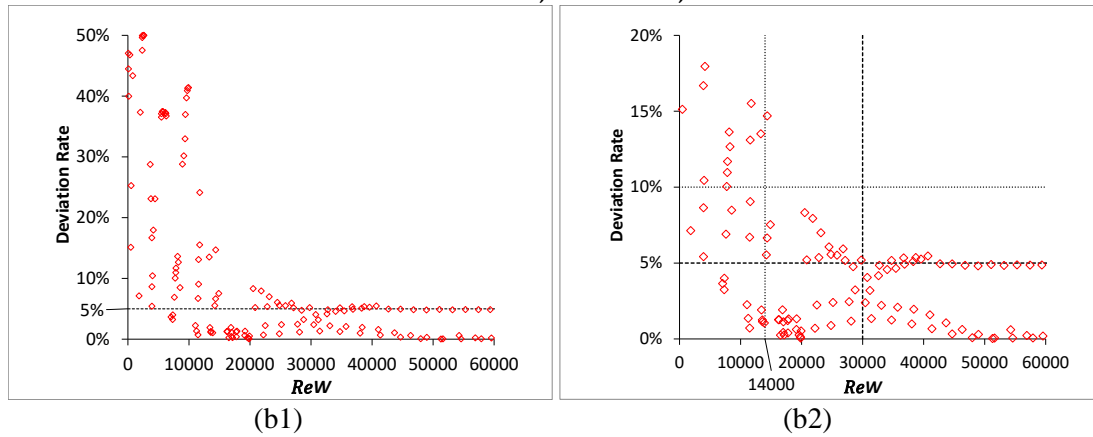
Similar to the assessment of the averaged wind velocity, the quantitative evaluation based on pollutant dispersion also needed to be conducted. The deviation rate of concentration was calculated as:

$$DR = \left| \frac{K_{Re_i} - K_{Re_j}}{K_{Re_i}} \right| \quad (14)$$

where K is the non-dimensional concentration according to changes in the Re and Re_i , and Re_j is the different Re levels.



$Z = 0 - 0.3\text{ m}, X = 0.3\text{ m}, Y = 0$



$Z = 0 - 0.3\text{ m}, X = -0.1\text{ m}, Y = 0$

Fig. 9 DR variations of the non-dimensional concentration with changes to the Re_H and Re_W . (a1) and (a2) The outdoor environment against the Re_H (b1) and (b2) and the indoor environment against the Re_W . (a1) and (b1) are amplified in (a2) and (b2).

Fig. 9 displays the concentration results of the DR varied with the Re_H and Re_W of outdoor and indoor conditions, respectively. Similar to the wind velocity results, the DR values of dimensionless concentration also showed a decreasing trend with an increasing Re and a sharp drop occurred when the Re was over a certain value. This revealed that a critical Re value exists in the pollutant dispersion fields. Over this value, the dimensionless concentration dispersion will vary within a small range with the Re . Regarding the DR values below 5%, for outdoor the environment, the Re_H value was slightly larger than the dimensionless wind velocity, which was 7.9×10^4 with $U_{ref} = 1 \text{ m/s}$. However, because of the more complex indoor pollutant distribution, the critical Re_W value for the indoor environments was much larger than the velocity fields to reach a DR below 5% that was up to 3.0×10^4 with $U_{ref} = 3 \text{ m/s}$. If the critical indication of the DR was extended to 10%, the result of the DR for the outdoor and indoor concentrations will agree with the velocity field, where was $Re_H > 4.8 \times 10^4$ and $Re_W > 1.4 \times 10^4$. These differences reveal that the concentration fields need more rigorous requirements to reach the Re -independence situation than the velocity fields; also, it further indicates that two sets of critical Re should be considered in coupled indoor and outdoor problems.

5.1.3 ACH and re-entry ratio

In addition to the velocity and concentration fields, two more parameters were used to evaluate the critical Re value for the flow and dispersion in coupled outdoor and indoor environments. As aforementioned, the tracer gas decay method was used to determine the ventilation rate and indicate the pollutant dispersion in a coupled indoor and outdoor environment (namely, using the parameter re-entry ratio).

Fig. 10 shows the mean dimensionless ventilation rates through a single opening in each room with a changing Re_W , where $(ACH)^*$ is defined as:

$$(ACH)^* = \frac{ACH}{U_{ref}} \cdot \frac{V}{A_W} \quad (15)$$

where U_{ref} is the referenced wind velocity (m/s), V is the volume of the room (m^3), and A_W is the area of the window (m^2). As shown in Fig. 10, two observations can be made. First, the dimensionless ventilation rate does not have the linear associations with the Re_W . When the Re_W reached a particular value, the results of the ventilation rates of each room concentrated into a narrow region numerically, as shown in the dashed circle in Fig. 10. This narrow region may be characteristic of the ventilation rate of the room in the present study. Also, it can be concluded that when the Re_W is larger than a critical value, the ventilation rate of the room can be independent of the Re . Then, the $(ACH)^*$ of the case with the $Re_W = 0.2 \times 10^4$ ($U_{ref} = 0.2 \text{ m/s}$) and 0.6×10^4 ($U_{ref} = 0.6 \text{ m/s}$) deviated obviously from cases with larger Re for most rooms. This illustrates that, for an isolated building, an Re_W equal to 1.0×10^4 is sufficient to predict the ventilation rate of the room between outdoor and indoor environments using the tracer gas decay method.

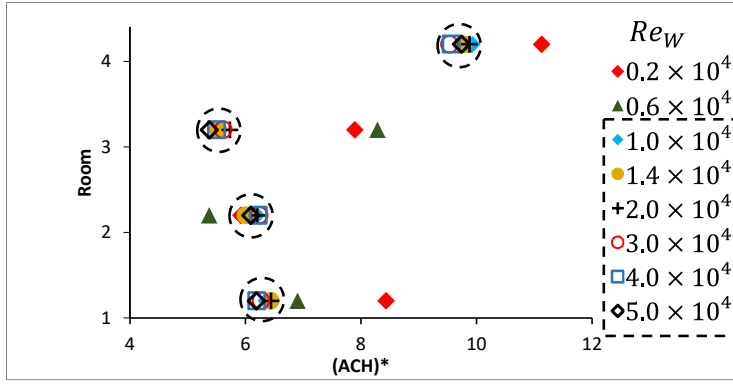


Fig. 10 $(ACH)^*$ values of each room with different Re_W .

Apart from the ACH, another indicator, the re-entry ratio, was also used to assess the Re -independence problem between the indoor and outdoor environments. The re-entry ratio was proposed by Ai and Mak [5] and defined as the fraction of the exhaust air from the source room that re-enters another room in the CFD simulations. According to this definition, the re-entry ratio in the present study was calculated by:

$$R_k = \frac{C_{i-j T_1}}{C_{i T_0} - C_{i T_1}} \cdot \frac{V_j}{V_i} \quad (16)$$

where $C_{i-j T_1}$ is the measured concentration (g/m^3) of the tracer gas in the re-entered room at time T_1 , $C_{i T_0}$ is the concentration (g/m^3) of the source room at the beginning, $C_{i T_1}$ is the concentration (g/m^3) of the source room at time T_1 , and V_i and V_j are the volumes of the source and re-entered room (m^3), respectively.

When the source was located in R2 as an example, the R_k of the R1 is shown in Fig. 11. When the Re_W was below 1.4×10^4 , R_k was elevated with the increase of the Re_W from 1.8% to 7.7%, representing a very large accretion. However, when the Re_W exceeded 1.4×10^4 , the R_k discrepancies became smaller, and the averaged value with the Re_W from 1.4×10^4 to 5.0×10^4 was 8.2%; the R_k fluctuated around 8.2% up to 6%. The results manifest that the predicted re-entry ratio by the CFD simulations also demonstrates the feature of independence on the Re after the Re_W exceeded a particular value in the isolated building situation.

Although, when the Re_W was 1.4×10^4 , the detailed concentration field showed 10% of the deviation rate as discussed in section 5.1.2. This can also be termed as the basic critical value in an indoor environment, because the general pollutant transportation was analogous to the Re_W over 3.0×10^4 as the results of the $(ACH)^*$ and R_k revealed. Note that, the results of the ventilation rates and re-entry ratios may only be suitable for the single-sided ventilation. Under cross-ventilation or other situations, further research should be conducted.

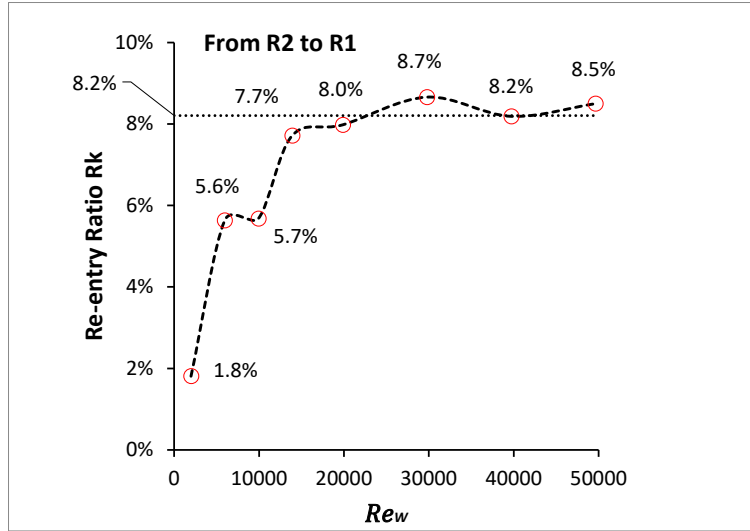


Fig. 11 Re-entry ratio R_k from R2 to R1 with increasing Re_w .

5.2 Building arrays

This section intends to further examine the flow structure and pollutant dispersion Re -independence in a more complex environment.

5.2.1 Airflow field

Fig. 12(2) shows the dimensionless mean wind velocity (U/U_{ref}) of four vertical lines in the building arrays, the upper two figures are the outdoor velocities and the lower two are the indoor velocities. For comparison, the same line positions for an isolated building are also shown in Fig. 12(1). Similar to the wind field of an isolated building, when the Re_H was above 4.8×10^4 and the Re_w was over 0.6×10^4 ($U_{ref} > 0.6 \text{ m/s}$), the differences for both the outdoor and indoor wind velocities with changes in the Re became negligible. However, since the upstream building arrays dramatically changed the flow field around the target building, diverse wind distributions occurred on the roof of the building. Additionally, for the indoor airflow field, the overall velocity was smaller compared to the isolated building. Further, the discrepancies between the wind fields of $U_{ref} < 0.6 \text{ m/s}$ and $U_{ref} > 0.6 \text{ m/s}$ for both the outdoor and indoor environments were diminished relative to the isolated building. This may be attributed the fact that the upstream building arrays functioned as a roughness element for the boundary layer, making the inlet wind more uniformly turbulent than in the isolated building situation. Fig 13 displays the DR results varied with the Re_H and Re_w for the outdoor and indoor environments, respectively. The Re criteria in the building arrays that retained the DR wind velocity less than 5% remained identical to the isolated building situation, that is $Re_H = 4.8 \times 10^4$ and $Re_w = 1.4 \times 10^4$. In addition, Fig. 13 also demonstrates the lower airflow velocity deviation rates relative to the isolated building DR distribution. This further implies that the regular upstream building arrays narrow the differences between the Re -dependent and Re -independent flow fields.

An isolated building

Building arrays

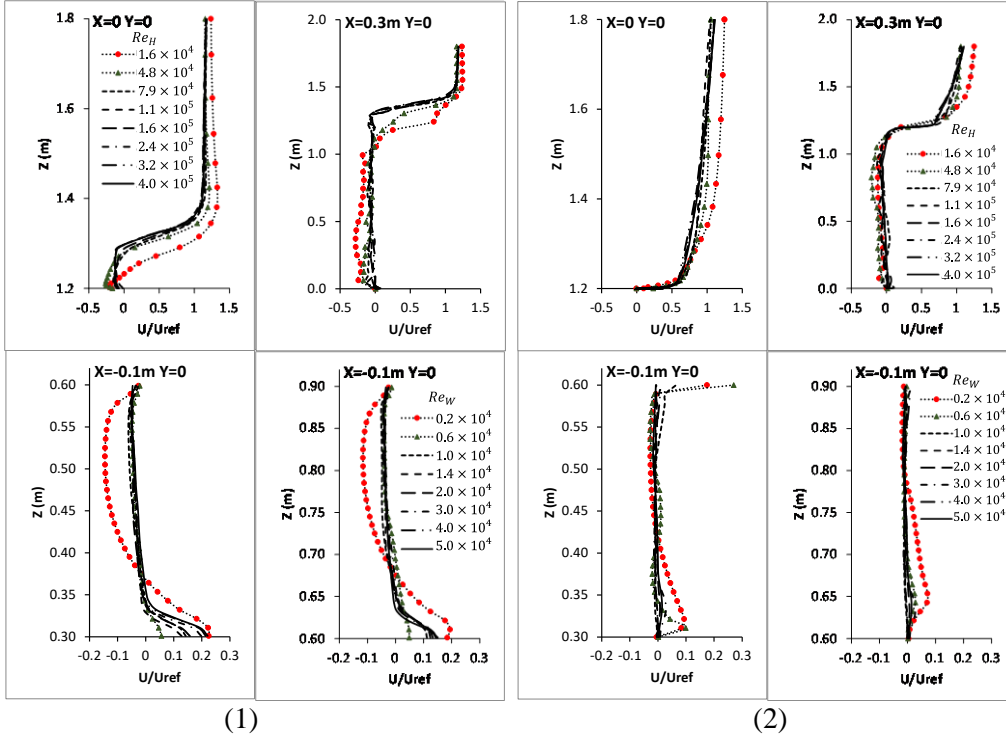
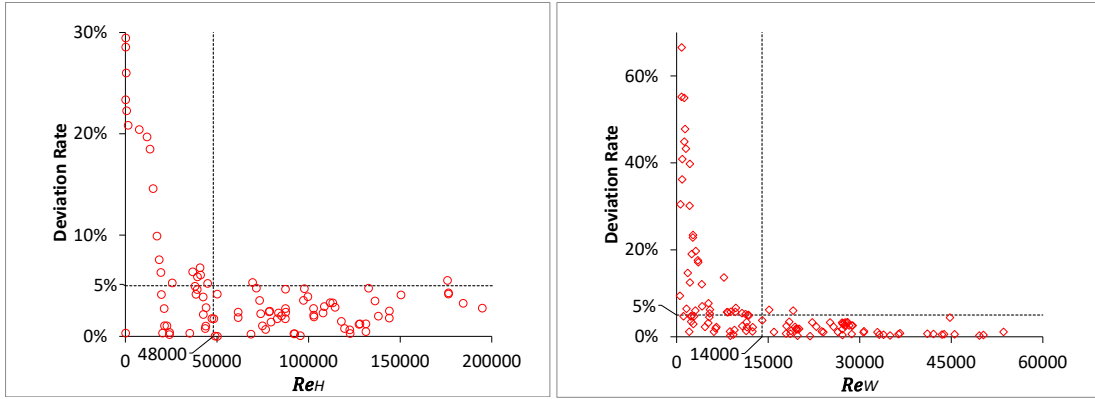


Fig. 12 Comparisons of the non-dimensional velocity on the outdoor and indoor environments of the (1) isolated building and (2) the building arrays.



(1) $Z = 1.2 - 1.8 \text{ m}, X = 0, Y = 0$

(2) $Z = 0.6 - 0.9 \text{ m}, X = 0.1 \text{ m}, Y = 0$

Fig. 13 DR variations of the averaged non-dimensional velocity with changes in the Re_H and Re_W . (1): The outdoor environment against the Re_H , and (2) the indoor environment against the Re_W .

5.2.2 Concentration field

To predict the pollutant dispersion field in the building arrays, the source room was set in Room 4 (R4) with the tracer gas CO_2 . During the sampling interval, the tracer gas was primarily transported downwards into Room 3 (R3) and separated around the target building. Fig. 14 displays the comparisons of the dimensionless concentration on the outdoor and indoor environments at four lines in both the vertical ($Y = 0$) and horizontal directions ($Z = 0.75 \text{ m}$). For the pollutant dispersion on the windward side of the target building, the differences in concentration results with increasing Re_H were not very large except for the noticeable overestimations of the results for $Re_H < 4.8 \times 10^4$ ($U_{ref} < 0.6 \text{ m/s}$). The discrepancies diminished when the Re_H was greater than 7.9×10^4 ($U_{ref} = 1.0 \text{ m/s}$), as shown in Fig. 14(1). The pollutant dispersion values on the leeward side were much lower than the windward side,

as shown in Fig. 14(2). Even with such small concentration values, the differences were mainly revealed by the results of $Re_H < 1.1 \times 10^5$ ($U_{ref} < 1.4$ m/s). For the indoor environment, as shown in Figs. 14(3) and (4), the pollutant distribution displayed similar patterns to the leeward side dispersion. Substantial discrepancies were found from Re_W values smaller than 1.4×10^4 (U_{ref} less than 1.4 m/s) in both the vertical and horizontal directions. When the Re_W was greater than 2×10^4 , the disparities declined and the distribution patterns of the dimensionless concentrations remained comparable.

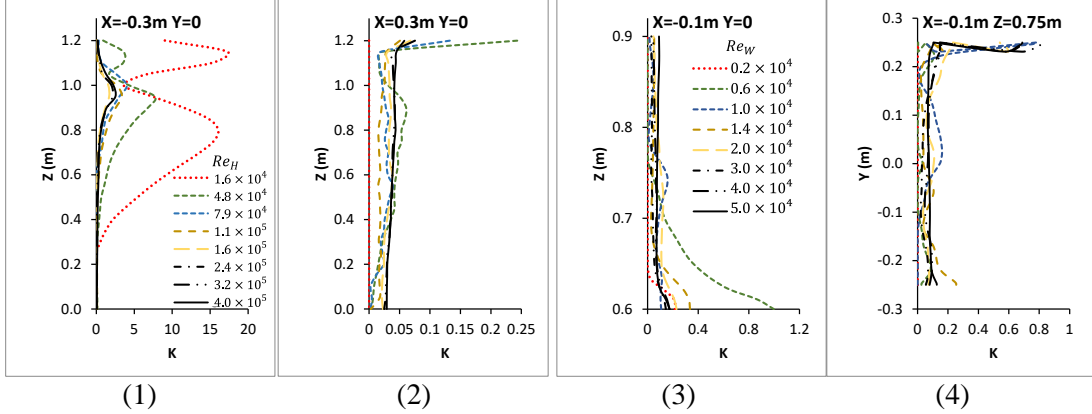
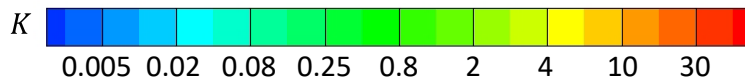
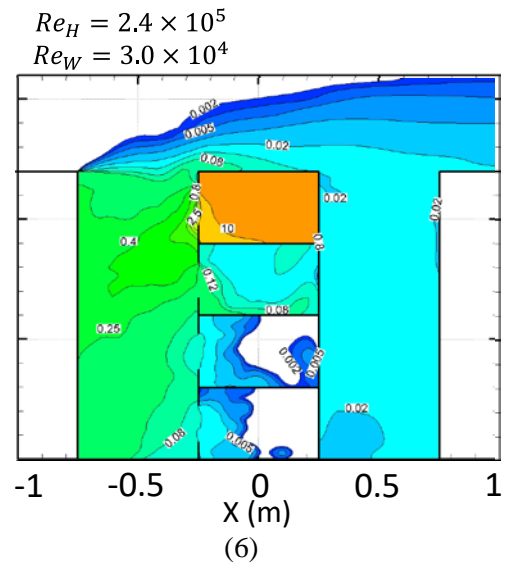
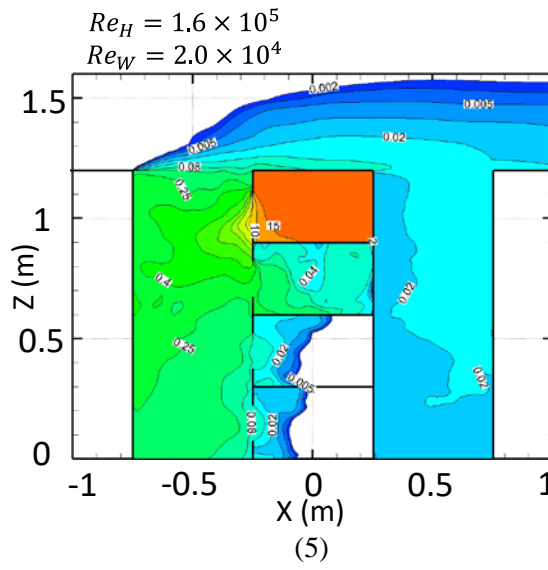
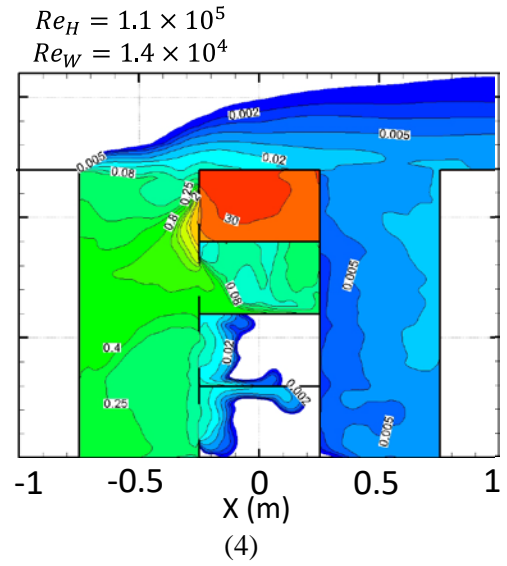
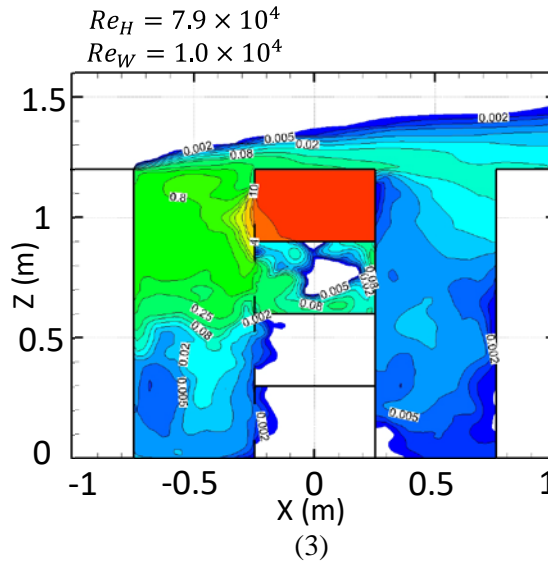
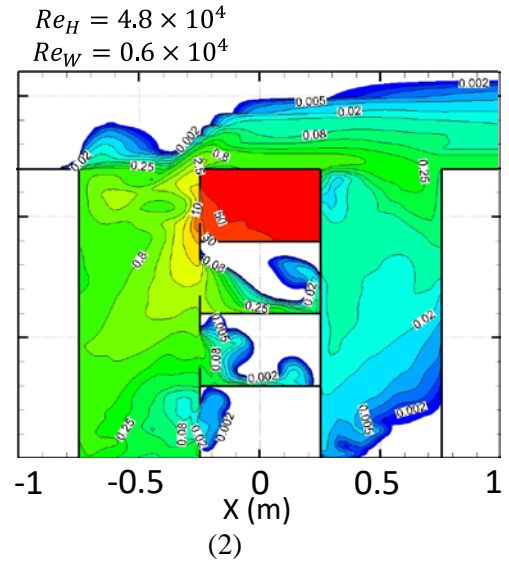
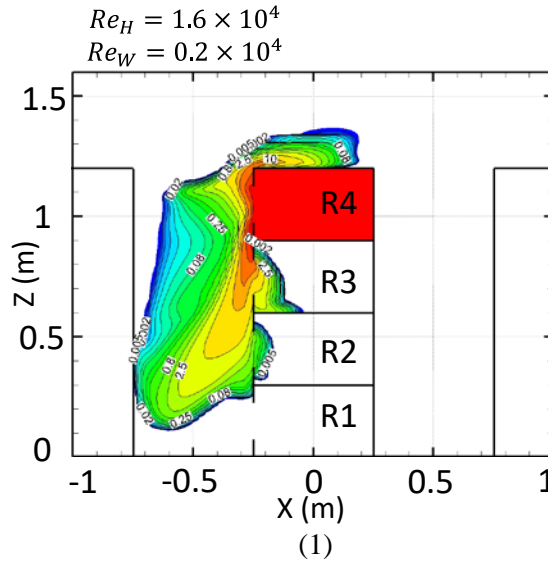


Fig. 14 Comparisons of the non-dimensional concentrations on the outdoor and indoor environments at lines in the vertical ($Y = 0$) and horizontal plane ($Z = 0.75$ m). (1, 2) Concentration distributions for the outdoor field, and (3, 4) concentration distributions for the indoor field.

Complementary investigations are shown in Fig. 15, that demonstrate the dimensionless concentration fields on the vertical plane $Y = 0$ with increasing Re_H and Re_W . The results below 0.001 are not shown in the figures and the room numbers are shown in Fig. 15(1). After the decay period, it was clearly demonstrated that for the outdoor places, pollutants released from Room 4 (R4) concentrated on the windward side of the target building and resulted in much higher K values compared to the others when the Re_H was less than 4.8×10^4 . With an increase in the Re_H , the pollutant dispersion fields became increasingly analogous and had basically identical K values, as shown in Figs. 15(3)–(8). For the leeward side of the building, the pollutants of the Re_H equal to 1.6×10^4 and 4.8×10^4 demonstrated opposite distribution fields, the tracer gas of $Re_H = 1.6 \times 10^4$ barely transported to the leeward side of the target building with this decay period; while $Re_H = 4.8 \times 10^4$ revealed overvalues for K on the leeward side. The pollutant fields of Re_H equal to 7.9×10^4 and 1.1×10^5 also displayed slight underestimations on the leeward side of the building relative to the results of $Re_H > 1.1 \times 10^5$. Deviations in the pollutant concentration fields were also detected on the roof of the building, when the Re_H was lower than 4.8×10^4 , the concentration results showed overestimations and irregular stratifications of the tracer gas. For Re_H over 4.8×10^4 , the stratifications of the pollutants became more stable and the discrepancies were eliminated. For the indoor places, the results agreed with the isolated building situation. When the Re_W reached 1.4×10^4 , the indoor pollutant dispersion remained almost unchanged. Therefore, for the pollutant distribution in the building arrays with coupled outdoor and indoor fields, the critical values conducted from the isolated building situation remained authentic, with an Re_H over 4.8×10^4 for the outdoor environments and an Re_W over 1.4×10^4 for the indoor environments.





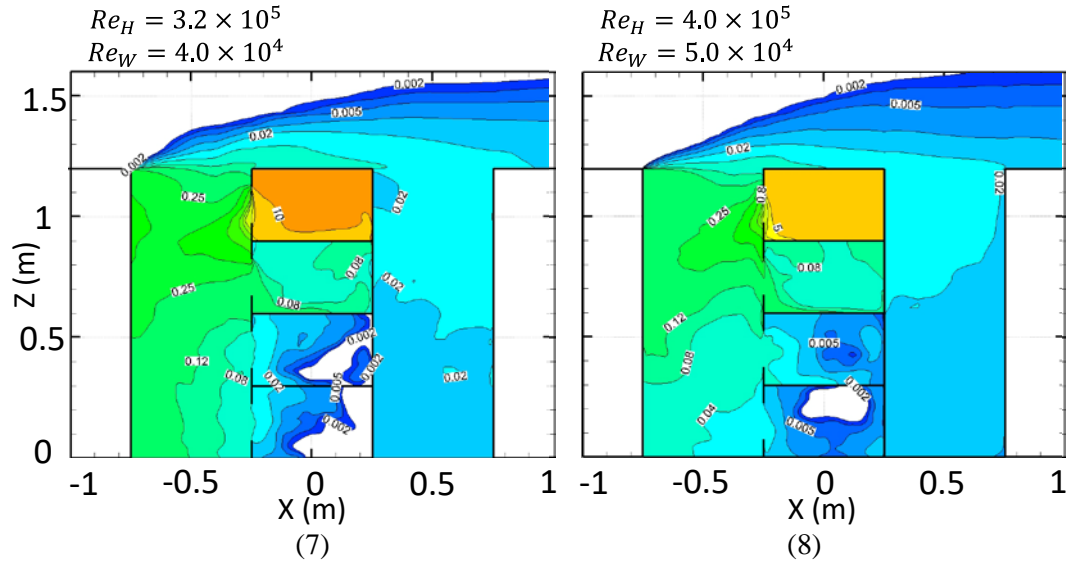
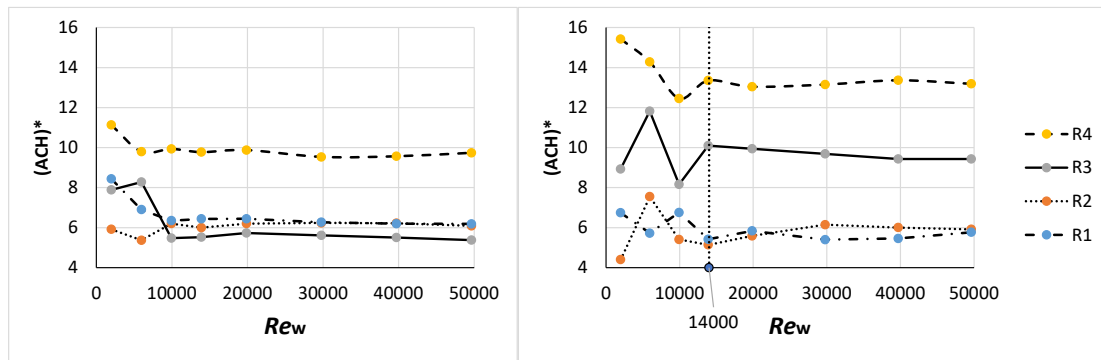


Fig. 15 Comparisons of the non-dimensional concentration fields on the vertical plane $Y = 0$ for the outdoor and indoor environments with variations in the Re_H and Re_W .

5.2.3 ACH and re-entry ratio

The tracer gas decay method was also used to predict the ventilation rate for each room in the building arrays and the dimensionless ventilation rates were calculated using equation (15) as described in section 5.1.3. Fig. 16 shows the dimensionless ventilation rates $(ACH)^*$ with the increasing Re_W for both the isolated building and building arrays, respectively. Since the surrounding buildings dramatically changed the airflow pattern around the target building, the ventilation rate results for each room in building arrays varied greatly comparing to the room in the isolated building. First, the ventilation rates in Room 3 (R3) and Room 4 (R4) greatly accelerated relative to the isolated building. Especially for R3, in an isolated building, the $(ACH)^*$ for R3 was lower than R1 and R2 when the Re_W was over 1.0×10^4 ; however, the R3 ventilation rate almost doubled in the building arrays. Then, in the building arrays, the $(ACH)^*$ became essentially constant with Re_W over 1.4×10^4 , while in the isolated building, Re_W up to 1.0×10^4 was sufficient to predict stable ventilation rates for each room. Therefore, in the building arrays, the Re based on the window height should be over 1.4×10^4 to predict reliable ventilation rates.



(1) an isolated building

(2) building arrays

Fig. 16 $(ACH)^*$ values for each room with increasing Re_W for the isolated building and the building arrays.

Because the ventilation performance significantly changed in each room of the building arrays, the re-entry ratio (R_k) for each room was also intensely altered. In this section, the source room was set in Room 4 (R4), Fig. 17 demonstrates the R_k for R3. With the increase of the Re_W , the R_k first rose and then became reduced around 2.4%. The peak 5.6% value occurred with the Re_W around 1.0×10^4 and was more than twice the stable value. This implies that over-

evaluation of the re-entry ratio will occur when the Re is below the criterion, that was 1.4×10^4 in the building arrays.

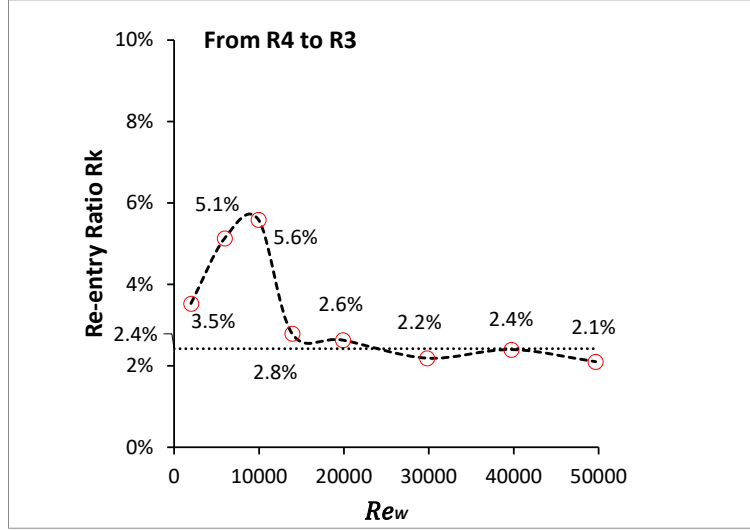


Fig. 17 Re-entry ratio R_k from R4 to R3 with increasing Re_w .

6. Conclusions

This study conducted a comprehensive numerical simulations using referenced wind velocity variations from 0.2 m/s to 5 m/s (Re_H from 1.6×10^4 to 4.0×10^5 , Re_w from 0.2×10^4 to 5.0×10^4) by the CFD method to investigate the Re -independence of flow and dispersion in coupled outdoor and indoor environments. Four parameters were used to assess the similarity of the flow patterns, including the non-dimensional air velocity, pollutant concentrations, ventilation rates, and the re-entry ratio for both an isolated building and building arrays. This study also compared the different results of the four parameters between an isolated building and building arrays. The conclusions are summarized as follows:

- (1) For both the isolated building and building arrays, the Re -independence criteria were different between the outdoor and indoor environments. The outdoor conditions can reach the Re -independent status at a smaller Re than the indoor area based on the same referenced wind velocity on the building height.
- (2) Taking the deviation rate (DR) of the dimensionless velocity below 5% as the critically quantitative assessment, $Re_H = 4.8 \times 10^4$ based on the building height and $Re_w = 1.4 \times 10^4$ based on the window height are recommended as the criteria for outdoor and indoor environments to predict the airflow fields, respectively.
- (3) The Re -independent requirement for pollutant concentration was more difficult to meet than the flow fields. Taking the DR of the dimensionless concentration below 5% as the critical assessment, Re_H reached 7.9×10^4 and Re_w was 3.0×10^4 to reach the requirement. If the DR was enlarged to 10%, the criteria for the Re_H and Re_w of the pollutant dispersion were the same as the velocity fields in both the isolated building and building arrays.
- (4) For the non-dimensional ventilation rates in each room, the critical values for the isolated buildings and building arrays were Re_w of 1.0×10^4 and 1.4×10^4 , respectively. For the re-entry ratio, the Re_w criterion for both the isolated buildings and building arrays was 1.4×10^4 .

Despite the obtained findings, the limitations of this study have to be revealed. First, this study only considered the isothermal conditions, but the buoyancy effect is an important driving force for natural ventilation especially when the wind speed is low. Second, this study only used generic building and window geometries, but real urban buildings and their surroundings are much more complicated. Third, this study used relatively large window openings and

considered only single-sided ventilation, but real buildings have different shapes and numbers of windows. Fourth, this study examined only the perpendicular wind direction, but other wind directions would create very different ventilation performances. All these factors could influence the Re -independence criteria suggested in this study, and this will be explored in our future studies.

Acknowledgement

The author(s) disclose the following financial support for research, authorship, and/or publication of this article: This work was supported by a PhD studentship funded by Hong Kong Polytechnic University.

References

1. Gao, N.P., Niu, J.L., Perino, M. and Heiselberg, P., 2008. *The airborne transmission of infection between flats in high-rise residential buildings: tracer gas simulation*. Building and Environment, 43(11), pp.1805-1817.
2. Niu, J.L., and Tung, T.C., 2008. *On-site quantification of re-entry ratio of ventilation exhausts in multi-family residential buildings and implications*. Indoor air, 18(1), pp.12-26.
3. Ai, Z.T. and Mak, C.M., 2014. *A study of interunit dispersion around multistory buildings with single-sided ventilation under different wind directions*. Atmospheric environment, 88, pp.1-13.
4. Ai, Z.T. and Mak, C.M., 2016. *Large eddy simulation of wind - induced interunit dispersion around multistory buildings*. Indoor air, 26(2), pp.259-273.
5. Ai, Z.T., Mak, C.M. and Niu, J.L., 2013. *Numerical investigation of wind - induced airflow and interunit dispersion characteristics in multistory residential buildings*. Indoor air, 23(5), pp.417-429.
6. Ai, Z.T. and Mak, C.M., *Large-eddy Simulation of flow and dispersion around an isolated building: Analysis of influencing factors*. Computers & Fluids, 2015. **118**(Supplement C): p. 89-100.
7. Cui, D.J., Mak, C.M., Kwok, K.C.S. and Ai, Z.T., 2016. *CFD simulation of the effect of an upstream building on the inter-unit dispersion in a multi-story building in two wind directions*. Journal of wind engineering and industrial aerodynamics, 150, pp.31-41.
8. Dai, Y.W., Mak, C.M. and Ai, Z.T., *Computational fluid dynamics simulation of wind-driven inter-unit dispersion around multi-storey buildings: Upstream building effect*. Indoor and Built Environment. 0(0): p. 1420326X17745943.
9. Mu, D., Gao, N.P. and Zhu, T., 2016. *Wind tunnel tests of inter-flat pollutant transmission characteristics in a rectangular multi-storey residential building, part A: effect of wind direction*. Building and Environment, 108, pp.159-170.
10. Mu, D., Shu, C., Gao, N.P. and Zhu, T., 2017. *Wind tunnel tests of inter-flat pollutant transmission characteristics in a rectangular multi-storey residential building, part B: Effect of source location*. Building and Environment, 114, pp.281-292.
11. Cao, S.J. and Meyers, J., *On the construction and use of linear low-dimensional ventilation models*. Indoor Air, 2012. **22**(5): p. 427-441.
12. Cao, S.J., Cen, D.D., Zhang, W.R. and Feng, Z.B., 2017. *Study on the impacts of human walking on indoor particles dispersion using momentum theory method*. Building and Environment, 126, pp.195-206.
13. Handbook, A., *ASHRAE Handbook-Fundamentals*. Atlanta, GA, 2009.
14. Yu, I.T., Li, Y., Wong, T.W., Tam, W., Chan, A.T., Lee, J.H., Leung, D.Y. and Ho, T., 2004. *Evidence of airborne transmission of the severe acute respiratory syndrome virus*. New England Journal of Medicine, 350(17), pp.1731-1739.

15. Meroney, R.N., 2004. *Wind tunnel and numerical simulation of pollution dispersion: a hybrid approach*. Paper for Invited Lecture at the Croucher Advanced Study Institute, Hong Kong University of Science and Technology, pp.6-10.
16. Snyder, W.H., *Guideline for fluid modeling of atmospheric diffusion*. Vol. 81. 1981: Environmental Sciences Research Laboratory, Office of Research and Development, US Environmental Protection Agency.
17. Blocken, B., *50 years of Computational Wind Engineering: Past, present and future*. Journal of Wind Engineering and Industrial Aerodynamics, 2014. **129**: p. 69-102.
18. Ai, Z.T. and Mak, C.M., *Potential use of reduced-scale models in CFD simulations to save numerical resources: Theoretical analysis and case study of flow around an isolated building*. Journal of wind engineering and industrial aerodynamics, 2014. **134**: p. 25-29.
19. Uehara, K., Wakamatsu, S. and Ooka, R., *Studies on critical Reynolds number indices for wind-tunnel experiments on flow within urban areas*. Boundary-layer meteorology, 2003. **107**(2): p. 353-370.
20. Alessio, S., Briatore, L., Longhetto, A., d'Hieres, G.C. and Didelle, H., 1983. *Laboratory simulation of rotating atmospheric boundary layer flows over obstacles*. II Nuovo Cimento C, 6(4), pp.401-428.
21. Contini, D., Cesari, D., Donato, A. and Robins, A.G., 2009. *Effects of Reynolds number on stack plume trajectories simulated with small scale models in a wind tunnel*. Journal of Wind Engineering and Industrial Aerodynamics, 97(9-10), pp.468-474.
22. Saathof, P., Stathopoulos, T. and Dobrescu, M., *Effects of model scale in estimating pollutant dispersion near buildings*. Journal of Wind Engineering and Industrial Aerodynamics, 1995. **54**: p. 549-559.
23. Saathoff, P., Gupta, A., Stathopoulos, T. and Lazure, L., 2009. *Contamination of fresh air intakes due to downwash from a rooftop structure*. Journal of the Air & Waste Management Association, 59(3), pp.343-353.
24. Obasaju, E. and Robins, A., *Simulation of pollution dispersion using small scale physical models—an assessment of scaling options*, Urban Air Quality: Monitoring and Modelling. 1998, Springer. p. 239-254.
25. Cui, P.Y., Li, Z. and Tao, W.Q., *Investigation of Re-independence of turbulent flow and pollutant dispersion in urban street canyon using numerical wind tunnel (NWT) models*. International Journal of Heat and Mass Transfer, 2014. **79**: p. 176-188.
26. Cui, P.Y., Li, Z. and Tao, W.Q., *Numerical investigations on Re-independence for the turbulent flow and pollutant dispersion under the urban boundary layer with some experimental validations*. International Journal of Heat and Mass Transfer, 2017. **106**: p. 422-436.
27. Van Hooff, T. and Blocken, B., *Full-scale measurements of indoor environmental conditions and natural ventilation in a large semi-enclosed stadium: possibilities and limitations for CFD validation*. Journal of Wind Engineering and Industrial Aerodynamics, 2012. **104**: p. 330-341.
28. Cermak, J.E., Poreh, M., Peterka, J.A. and Ayad, S.S., *Wind tunnel investigations of natural ventilation*. Journal of transportation engineering, 1984. **110**(1): p. 67-79.
29. Liu, X.P., Niu, J.L., Perino, M. and Heiselberg, P., *Numerical simulation of inter-flat air cross-contamination under the condition of single-sided natural ventilation*. Journal of Building Performance Simulation, 2008. **1**(2): p. 133-147.
30. Liu, X.P., Niu, J.L., Kwok, K.C.S., Wang, J.H. and Li, B.Z., *Investigation of indoor air pollutant dispersion and cross-contamination around a typical high-rise residential building: Wind tunnel tests*. Building and Environment, 2010. **45**(8): p. 1769-1778.
31. Ramponi, R. and Blocken, B., *CFD simulation of cross-ventilation flow for different isolated building configurations: validation with wind tunnel measurements and analysis of physical and numerical diffusion effects*. Journal of Wind Engineering and Industrial Aerodynamics, 2012. **104**: p. 408-418.
32. Chen, Q.Y., *Ventilation performance prediction for buildings: A method overview and recent applications*. Building and environment, 2009. **44**(4): p. 848-858.

33. Ai, Z.T. and Mak, C.M., *Modeling of coupled urban wind flow and indoor air flow on a high-density near-wall mesh: Sensitivity analyses and case study for single-sided ventilation*. Environmental modelling & software, 2014. **60**: p. 57-68.
34. Ai, Z.T. and Mak, C.M., *Analysis of fluctuating characteristics of wind-induced airflow through a single opening using LES modeling and the tracer gas technique*. Building and environment, 2014. **80**: p. 249-258.
35. Hinze, J., *Turbulence*, (1975). New York, 1959.
36. Smagorinsky, J., *General circulation experiments with the primitive equations: I. The basic experiment*. Monthly weather review, 1963. **91**(3): p. 99-164.
37. Lilly, D.K., *A proposed modification of the Germano subgrid - scale closure method*. Physics of Fluids A: Fluid Dynamics, 1992. **4**(3): p. 633-635.
38. Fluent, 13.0 Theory Guide, Turbulence. ANSYS Inc., Canonsburg, PA, 2010.
39. Laussmann, D. and Helm, D., *Air change measurements using tracer gases: Methods and results. Significance of air change for indoor air quality*, in *Chemistry, Emission Control, Radioactive Pollution and Indoor Air Quality*. 2011, InTech.
40. Dascalaki, E., Santamouris, M., Argiriou, A., Helmis, C., Asimakopoulos, D.N., Papadopoulos, K. and Soilemes, A., *On the combination of air velocity and flow measurements in single sided natural ventilation configurations*. Energy and Buildings, 1996. **24**(2): p. 155-165.
41. Franke, J., *Best practice guideline for the CFD simulation of flows in the urban environment*. 2007: Meteorological Inst.
42. Leidl, B. and Schatzmann, M., *Cedval at hamburg university*. URL <http://www.mi.uni-hamburg.de/cedval>, 2010.
43. Dai, Y.W., Mak, C.M., Ai, Z.T., and Hang, J., 2018. *Evaluation of computational and physical parameters influencing CFD simulations of pollutant dispersion in building arrays*. Building and Environment, 137, pp.90-107.